

The Effect of Airflow on the Wavelength of Ripples on Icicles

K. Ueno and M. Farzaneh

NSERC/Hydro-Quebec/UQAC Industrial Chair on Atmospheric Icing of Power Network Equipment (CIGELE) and Canada Research Chair on Atmospheric Icing Engineering of Power Networks (INGIVRE) <http://www.cigele.ca> at the Universite du Quebec a Chicoutimi, Chicoutimi, QC, Canada

Abstract—Icicles are important in recent icing models. A numerical simulation of glaze icing in freezing rain with icicle growth by Makkonen has shown that when the air temperature is high enough for icicle growth, the total load may be much higher than at any other temperature. When an icicle grows, the latent heat released in the freezing of ice beneath the water film must be removed from the ice and water interface. The rate of heat loss from the surface to the air by thermal convection and evaporation controls the growth rate of the ice. In the icicle growth and wet accretion model, it is important to estimate the local heat transfer coefficient. In previous studies on the subject of ripple formation mechanisms on the surface of icicles, one of the authors herein showed that the change in the mean growth rate of icicle radius affects the magnitude of amplification rate for disturbances of the ice-water interface, but the characteristic wavelength of the ripples does not change. However, it was assumed in previous studies that there is no airflow around icicles. If we take into account natural or forced convection of the air, we have to consider airflow within the thermal boundary layer around icicles. In this paper, we extend the previous theoretical framework by taking into account the effect of airflow on the morphology of the ice-water interface.

I. INTRODUCTION

THE traditional approach in wet icing modeling has been to ignore the dynamics of the surface flow of unfrozen water [1]. Since the situation of wet growth is analogous to icicle growth, icicles have become an important aspect of icing models today. When there is a source of water at the root of the icicle, a water film forms on the icicle surface. The rate of heat loss from the ice-water interface to the environment through the water film controls the growth rate of the ice. One side of the water film is a water-air surface and the other side is growing ice. As a result of the instability of the ice-water interface, the flow in the water film may be changed depending on the morphology of ice. This means that two interfaces have to be dealt with, making this one of the more complicated moving boundary problems with phase transition.

When an icicle grows, we often observe ring-like ripples on the surface about one centimeter in wavelength. Recent theoretical research to explain the underlying dynamic instability that produces ripples is based on the assumption that ice is covered with the supercooled water film in the mean thickness h_0 , and that there is no airflow ahead of the ice surface, as shown in Fig. 1 (a) [2]-[4]. The thickness of the water film is given by $h_0 = [3\nu_l / (g \sin \theta) Q/l]^{1/3}$ [5], [6], where ν_l is the kinematic viscosity of water, g the gravitational acceleration, Q/l [(ml/h)/cm] the water supply

rate per width from the top, and θ is the inclination angle with respect to the horizontal plane. $h_0 \approx 100 \mu\text{m}$ for typical values of Q/l [7].

However, as indicated by the experimental observation that the increase in wind speed leads to an increase in the mean growth rate of icicle radius [7], heat transport can be greatly influenced by the presence of forced convection airflow. In order to clarify the effect of the enhancement of heat transfer due to air convection in the thermal boundary layer on the morphology of ice, we extend the previous two-dimensional model of ice growth under a supercooled water film flow to include a natural convection airflow adjacent to the ice surface. We assume that this flow occurs by buoyancy force, which arises by density difference due to latent heat released from the ice-water interface into the air close to the ice surface [8]. As a result, as shown in Fig. 1 (b), a rising thermal boundary layer is created ahead of the ice surface.

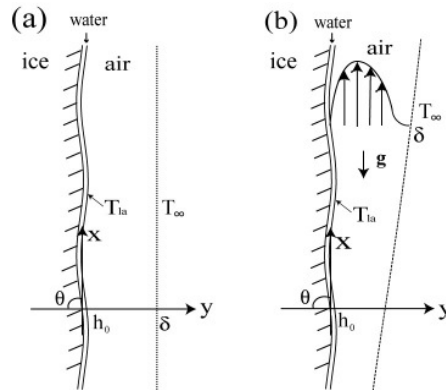


Fig. 1. (a) is the absence of airflow, (b) is the presence of a natural convection airflow. h_0 is the thickness of the water film. The air temperature is T_{la} at the water-air surface and T_∞ at a length δ .

In the absence of airflow, at the inclination angle of $\theta = \pi/2$, we derived a formula to determine the wavelength of ripples: $\lambda \approx 2\pi(a^2 h_0 Pe_l / 3)^{1/3}$, where $a = [\gamma / (\rho_l g)]^{1/2}$ is the capillary length associated with the surface tension γ of the ice-water interface [6], ρ_l , the density of water, and Pe_l , the Peclet number, which is the ratio of the heat transfer due to water flow to that due to thermal conduction in the water film. In previous studies [2]-[4], we assumed a linear air temperature profile ahead of the water-air surface: $\bar{T}_a = T_{la}$ at the water-air surface and $\bar{T}_a = T_\infty$ at a length scale δ , as shown in Fig. 1. (a), and the latent heat was assumed to be

transported in the air by conduction only. We showed that the length scale δ only appears in the ice growth rate $\bar{V} = -K_a T_\infty / (L\delta)$, but the wavelength λ of ripples is not relevant to δ . Here K_a is the thermal conductivity of the air and L , the latent heat per unit volume [4]. However, δ was an unknown parameter and the physical meaning of this length scale was not given. When we take into account natural convection of the air around icicles, δ is regarded as the thickness of the thermal boundary layer [9]. If δ is also important in determining the wavelength of ripples, the above formula for λ would be modified to include δ . In this paper, assuming a mean air velocity profile and a mean air temperature profile in the boundary layer as shown in Figs. 2 (a) and (b), respectively, a linear stability analysis for a disturbance of the ice-water interface during ice growth is performed.

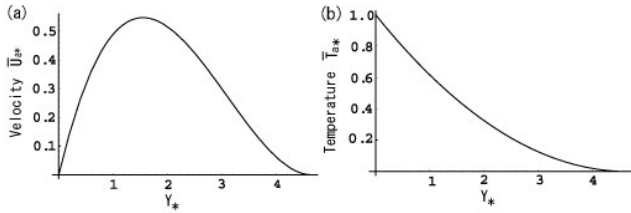


Fig. 2. (a) Dimensionless air velocity profile \bar{U}_{a*} , (b) Dimensionless air temperature profile \bar{T}_{a*} with respect to dimensionless coordinate Y_* .

II. THEORY

A. Governing equations

We consider the laminar natural convection flow over semi-infinite ice covered with a supercooled water film as shown in Fig. 1 (b). Using the stream function ψ_l , the velocity components in the x and y directions in the water film, $u_l = \partial\psi_l / \partial y$ and $v_l = -\partial\psi_l / \partial x$, are governed by the Navier-Stokes equations driven by gravity force and the continuity equation [5], [6]:

$$\frac{\partial u_l}{\partial t} + u_l \frac{\partial u_l}{\partial x} + v_l \frac{\partial u_l}{\partial y} = -\frac{1}{\rho_l} \frac{\partial p_l}{\partial x} + \nu_l \left(\frac{\partial^2 u_l}{\partial x^2} + \frac{\partial^2 u_l}{\partial y^2} \right) - g \sin \theta, \quad (1)$$

$$\frac{\partial v_l}{\partial t} + u_l \frac{\partial v_l}{\partial x} + v_l \frac{\partial v_l}{\partial y} = -\frac{1}{\rho_l} \frac{\partial p_l}{\partial y} + \nu_l \left(\frac{\partial^2 v_l}{\partial x^2} + \frac{\partial^2 v_l}{\partial y^2} \right) - g \cos \theta, \quad (2)$$

$$\frac{\partial u_l}{\partial x} + \frac{\partial v_l}{\partial y} = 0, \quad (3)$$

where $\nu_l = 1.8 \times 10^{-6} \text{ m}^2/\text{s}$ and $\rho_l = 1.0 \times 10^3 \text{ kg/m}^3$ are the kinematic viscosity and density of water, g , the gravitational acceleration, and p_l , the pressure in the water. The equations for the temperatures in the ice T_s and water T_l are given by

$$\frac{\partial T_s}{\partial t} = \kappa_s \left(\frac{\partial^2 T_s}{\partial x^2} + \frac{\partial^2 T_s}{\partial y^2} \right), \quad (4)$$

$$\frac{\partial T_l}{\partial t} + u_l \frac{\partial T_l}{\partial x} + v_l \frac{\partial T_l}{\partial y} = \kappa_l \left(\frac{\partial^2 T_l}{\partial x^2} + \frac{\partial^2 T_l}{\partial y^2} \right), \quad (5)$$

where $\kappa_s = 1.15 \times 10^{-6} \text{ m}^2/\text{s}$ and $\kappa_l = 1.33 \times 10^{-7} \text{ m}^2/\text{s}$ are the thermal diffusivities of the ice and water, respectively.

Employing the Boussinesq approximation, the air velocity components in the x and y directions, $u_a = \partial\psi_a / \partial y$ and $v_a = -\partial\psi_a / \partial x$, and air temperature T_a are governed by the Boussinesq equations [6]:

$$\frac{\partial u_a}{\partial t} + u_a \frac{\partial u_a}{\partial x} + v_a \frac{\partial u_a}{\partial y} = -\frac{1}{\rho_\infty} \frac{\partial(p_a - p_{a0})}{\partial x} + \nu_a \left(\frac{\partial^2 u_a}{\partial x^2} + \frac{\partial^2 u_a}{\partial y^2} \right) + g\beta(T_a - T_\infty) \sin \theta, \quad (6)$$

$$\frac{\partial v_a}{\partial t} + u_a \frac{\partial v_a}{\partial x} + v_a \frac{\partial v_a}{\partial y} = -\frac{1}{\rho_\infty} \frac{\partial(p_a - p_{a0})}{\partial y} + \nu_a \left(\frac{\partial^2 v_a}{\partial x^2} + \frac{\partial^2 v_a}{\partial y^2} \right) + g\beta(T_a - T_\infty) \cos \theta, \quad (7)$$

$$\frac{\partial u_a}{\partial x} + \frac{\partial v_a}{\partial y} = 0, \quad (8)$$

$$\frac{\partial T_a}{\partial t} + u_a \frac{\partial T_a}{\partial x} + v_a \frac{\partial T_a}{\partial y} = \kappa_a \left(\frac{\partial^2 T_a}{\partial x^2} + \frac{\partial^2 T_a}{\partial y^2} \right), \quad (9)$$

where ψ_a is the air stream function, p_a is the air pressure, p_{a0} , the static air pressure, ρ_∞ , the air density at temperature T_∞ , and $\nu_a = 1.3 \times 10^{-5} \text{ m}^2/\text{s}$ and $\beta = 3.7 \times 10^{-3} \text{ K}^{-1}$ are the kinematic viscosity and the volumetric coefficient of thermal expansion of the air, and $\kappa_a = 1.87 \times 10^{-5} \text{ m}^2/\text{s}$ is the thermal diffusivities of air.

B. Boundary conditions

First, we consider the hydrodynamic boundary conditions. Both water velocity components $u_l = \partial\psi_l / \partial y$ and $v_l = -\partial\psi_l / \partial x$ at a disturbed ice-water interface, $y = \zeta(t, x)$, must satisfy

$$u_l |_{y=\zeta} = 0, \quad v_l |_{y=\zeta} = 0. \quad (10)$$

The kinematic condition at a disturbed water-air surface, $y = \xi(t, x)$, is

$$\frac{\partial \xi}{\partial t} + u_l |_{y=\xi} \frac{\partial \xi}{\partial x} = v_l |_{y=\xi}. \quad (11)$$

At the water-air surface we impose the free shear stress:

$$\left. \frac{\partial u_l}{\partial y} \right|_{y=\xi} + \left. \frac{\partial v_l}{\partial x} \right|_{y=\xi} = 0, \quad (12)$$

and the normal stress including the stress induced by the surface tension $\gamma = 7.6 \times 10^{-2} \text{ N/m}$ of the water-air surface must balance the atmospheric pressure P_0 :

$$-p_l |_{y=\xi} + 2\rho_l \nu_l \left. \frac{\partial v_l}{\partial y} \right|_{y=\xi} - \gamma \frac{\partial^2 \xi}{\partial x^2} = -P_0. \quad (13)$$

For both air velocity components $u_a = \partial\psi_a / \partial y$ and $v_a = -\partial\psi_a / \partial x$ at the water-air surface and far away from the ice surface, we impose

$$u_a |_{y=\xi} = 0, \quad v_a |_{y=\xi} = 0, \quad u_a |_{y=\delta} = 0, \quad v_a |_{y=\delta} = 0. \quad (14)$$

Second, we consider the thermodynamic boundary conditions. The continuity of the temperature at a disturbed ice-water interface is

$$T_l |_{y=\zeta} = T_s |_{y=\zeta} = T_{sl} + \Delta T_{sl}, \quad (15)$$

where T_{sl} is the temperature at the flat ice-water interface and ΔT_{sl} is a deviation from it when the ice-water interface is disturbed. The heat conservation at the ice-water interface is

$$L\left(\bar{V} + \frac{\partial \zeta}{\partial t}\right) = K_s \frac{\partial T_s}{\partial y} \Big|_{y=\zeta} - K_l \frac{\partial T_l}{\partial y} \Big|_{y=\zeta}, \quad (16)$$

where $L = 3.3 \times 10^8$ J/m³ is the latent heat per unit volume, and $K_s = 2.22$ J/(m K s) and $K_l = 0.56$ J/(m K s) are the thermal conductivities of the ice and water, respectively. The continuity of the temperature at a disturbed water-air surface is

$$T_l \Big|_{y=\xi} = T_a \Big|_{y=\xi} = T_{la}, \quad (17)$$

where T_{la} is a temperature at the water-air surface. The heat conservation at the water-air surface is

$$-K_l \frac{\partial T_l}{\partial y} \Big|_{y=\xi} = -K_a \frac{\partial T_a}{\partial y} \Big|_{y=\xi}, \quad (18)$$

where $K_a = 0.024$ J/(m K s) is the thermal conductivity of the air. Far away from the ice surface the air temperature satisfies

$$T_a \Big|_{y=\delta} = T_\infty. \quad (19)$$

C. Perturbations

Since a ring-like structure encircles the icicles and there is no noticeable azimuthal variation on the surface of the icicles, it is sufficient to consider only one-dimensional perturbation in the x direction of the ice-water interface, $\zeta(t, x) = \zeta_k \exp[\sigma t + ikx]$, where k is the wave number and $\sigma = \sigma^{(r)} + i\sigma^{(i)}$, with $\sigma^{(r)}$ being the amplification rate and $v_p \equiv -\sigma^{(i)}/k$ being the phase velocity of the perturbation, and ζ_k is a small amplitude of the ice-water interface. We separate ξ , ψ_l , ψ_a , p_l , T_s , T_l and T_a into unperturbed steady fields and perturbed fields with prime, as follows: $\xi = h_0 + \xi'$, $\psi_l = \bar{\psi}_l + \psi'_l$, $\psi_a = \bar{\psi}_a + \psi'_a$, $p_l = \bar{p}_l + p'_l$, $T_s = \bar{T}_s + T'_s$, $T_l = \bar{T}_l + T'_l$ and $T_a = \bar{T}_a + T'_a$. We suppose that the respective perturbed parts are expressed as follows:

$$\begin{pmatrix} \xi'(t, x) \\ \psi'_l(t, x, y) \\ \psi'_a(t, x, y) \\ p'_l(t, x, y) \\ T'_s(t, x, y) \\ T'_l(t, x, y) \\ T'_a(t, x, y) \end{pmatrix} = \begin{pmatrix} \xi_k \\ F_l(y) \\ F_a(y) \\ \Pi_l(y) \\ g_s(y) \\ g_l(y) \\ g_a(y) \end{pmatrix} \exp[\sigma t + ikx], \quad (20)$$

where ξ_k , F_l , F_a , Π_l , g_s , g_l and g_a are the amplitudes of respective perturbations and are assumed to be in the order of ζ_k . The following calculation is based on a linear stability analysis taking into account only the first order of ζ_k .

D. Equations of unperturbed part in the air boundary layer

We introduce the following dimensionless variables:

$$X_* = x/L_0, \quad Y_* = Gr_a^{1/4} y/L_0 = y/\delta_0, \quad \bar{U}_{a*} = \bar{U}_a/u_{a0},$$

$\bar{V}_{a*} = Gr_a^{1/4} \bar{v}_a/u_{a0}$ and $\bar{T}_{a*} = (\bar{T}_a - T_\infty)/(T_{la} - T_\infty)$, where $Gr_a = g\beta\Delta T_a L_0^3/\nu_a^2$ is the Grashof number, $u_{a0} = \sqrt{g\beta\Delta T_a L_0}$, $\delta_0 = L_0 Gr_a^{-1/4} = [\nu_a^2 L_0/(g\beta\Delta T_a)]^{1/4}$, L_0 a characteristic dimension of the body, ΔT_a the temperature difference between the water-air surface and ambient air temperature. For example, the values of Gr_a , u_{a0} and δ_0 are 2.1×10^9 , 0.6 m/s and 4.6 mm, respectively, for $L_0 = 1$ m and $\Delta T_a = 10$ °C.

Applying the boundary layer approximation to the Boussinesq equations (6)-(9), $\bar{U}_{a*}(X_*, Y_*)$, $\bar{V}_{a*}(X_*, Y_*)$ and $\bar{T}_{a*}(X_*, Y_*)$ are governed by [6], [8]

$$\frac{\partial \bar{U}_{a*}}{\partial X_*} + \frac{\partial \bar{V}_{a*}}{\partial Y_*} = 0, \quad (21)$$

$$\bar{U}_{a*} \frac{\partial \bar{U}_{a*}}{\partial X_*} + \bar{V}_{a*} \frac{\partial \bar{U}_{a*}}{\partial Y_*} = \frac{\partial^2 \bar{U}_{a*}}{\partial Y_*^2} + \bar{T}_{a*} \sin \theta, \quad (22)$$

$$\bar{U}_{a*} \frac{\partial \bar{T}_{a*}}{\partial X_*} + \bar{V}_{a*} \frac{\partial \bar{T}_{a*}}{\partial Y_*} = \frac{1}{Pr_a} \frac{\partial^2 \bar{T}_{a*}}{\partial Y_*^2}, \quad (23)$$

where $Pr_a = \nu_a/\kappa_a$ is the Prandtl number of the air. Following the profile method [10], we assume the functional forms of $\bar{U}_{a*}(X_*, Y_*)$ and $\bar{T}_{a*}(X_*, Y_*)$ as follows:

$$\bar{U}_{a*}(X_*, Y_*) = u_{a0*} \frac{Y_*}{\delta_*} \left(1 - \frac{Y_*}{\delta_*}\right)^2, \quad (24)$$

$$\bar{T}_{a*}(X_*, Y_*) = \left(1 - \frac{Y_*}{\delta_*}\right)^2, \quad (25)$$

which satisfy the boundary conditions $\bar{U}_{a*}|_{Y_*=0} = 0$, $\bar{U}_{a*}|_{Y_*=\delta_*} = 0$, $\partial \bar{U}_{a*}/\partial Y_*|_{Y_*=\delta_*} = 0$ and $\bar{T}_{a*}|_{Y_*=0} = 1$, $\bar{T}_{a*}|_{Y_*=\delta_*} = 0$, $\partial \bar{T}_{a*}/\partial Y_*|_{Y_*=\delta_*} = 0$. The profiles of $\bar{U}_{a*}(X_*, Y_*)$ and $\bar{T}_{a*}(X_*, Y_*)$ are shown in Figs. 2 (a) and (b). From (21),

$$\bar{V}_{a*}(X_*, Y_*) = -\frac{u_{a0*} \delta_*}{16 X_*} \left[2 \left(\frac{Y_*}{\delta_*}\right)^2 - \left(\frac{Y_*}{\delta_*}\right)^4 \right]. \quad (26)$$

Substituting (24), (25) into (22) and (23) and integrating them, we obtain

$$u_{a0*} = 4 \left(\frac{5}{3}\right)^{1/2} \left(\frac{20}{21} + Pr_a\right)^{-1/2} (X_* \sin \theta)^{1/2}, \quad (27)$$

$$\delta_* \equiv \frac{\delta}{\delta_0} = 2 \cdot 15^{1/4} Pr_a^{-1/2} \left(\frac{20}{21} + Pr_a\right)^{1/4} \left(\frac{X_*}{\sin \theta}\right)^{1/4}. \quad (28)$$

Here we assume the thickness of the thermal boundary layer and that of velocity boundary layer to be the same order of δ , thus we put $Pr_a = 1.0$.

If we use the temperature profile (25), the continuity of heat flux at the ice-water interface and water-air surface yield

$$\bar{V} = \frac{K_a}{L} \frac{T_{sl} - T_\infty}{\delta_0} \bar{G}_{a^*}, \quad T_{la} = \frac{T_{sl} + \frac{K_a}{K_l} \frac{h_0}{\delta_0} T_\infty \bar{G}_{a^*}}{1 + \frac{K_a}{K_l} \frac{h_0}{\delta_0} \bar{G}_{a^*}}, \quad (29)$$

where $\bar{G}_{a^*} \equiv -\partial \bar{T}_{a^*} / \partial Y_* |_{Y_*=0} = 2 / \delta_*$. Since δ_* include the Prandtl number, \bar{G}_{a^*} depends on the Prandtl number. In the case of $\text{Pr}_a = 1.0$, we can estimate $\bar{G}_{a^*} = 0.43$ for $X_* = 1.0$ and $\theta = \pi / 2$.

E. Equations of perturbed part in the air boundary layer

Substituting $u_a = \bar{U}_a + u'_a = \bar{U}_a + \partial \psi'_a / \partial y$, $v_a = \bar{v}_a + v'_a = \bar{v}_a - \partial \psi'_a / \partial x$ and $T_a = \bar{T}_a + T'_a$ into the complete equations (6), (7) and (9), and introducing the following dimensionless variables: $x_* = x / \delta_0$, $Y_* = y / \delta_0$, $\bar{U}_{a^*} = \bar{U}_a / u_{a0}$, $\bar{v}_{a^*} = \bar{v}_a / u_{a0}$, $u'_{a^*} = u'_a / u_{a0} = \partial \psi'_{a^*} / \partial Y_*$, $v'_{a^*} = v'_a / u_{a0} = -\partial \psi'_{a^*} / \partial x_*$ and $T'_{a^*} = T'_a / (T_{la} - T_\infty)$, in the quasi-stationary approximation, we obtain the equations for ψ'_{a^*} and T'_{a^*} :

$$\begin{aligned} & \frac{1}{Gr_a^{1/4}} \left(\frac{\partial^4 \psi'_{a^*}}{\partial Y_*^4} + 2 \frac{\partial^4 \psi'_{a^*}}{\partial x_*^2 \partial Y_*^2} + \frac{\partial^4 \psi'_{a^*}}{\partial x_*^4} \right) \\ &= \bar{U}_{a^*} \left(\frac{\partial^3 \psi'_{a^*}}{\partial x_* \partial Y_*^2} + \frac{\partial^3 \psi'_{a^*}}{\partial x_*^3} \right) + \bar{v}_{a^*} \left(\frac{\partial^3 \psi'_{a^*}}{\partial Y_*^3} + \frac{\partial^3 \psi'_{a^*}}{\partial x_*^2 \partial Y_*} \right) \\ & - \frac{\partial \psi'_{a^*}}{\partial x_*} \left(\frac{\partial^2}{\partial x_*^2} + \frac{\partial^2}{\partial Y_*^2} \right) \bar{U}_{a^*} - \frac{\partial \psi'_{a^*}}{\partial Y_*} \left(\frac{\partial^2}{\partial x_*^2} + \frac{\partial^2}{\partial Y_*^2} \right) \bar{v}_{a^*} \\ & - \frac{1}{Gr_a^{1/4}} \left(\frac{\partial T'_{a^*}}{\partial Y_*} \sin \theta - \frac{\partial T'_{a^*}}{\partial x_*} \cos \theta \right), \end{aligned} \quad (30)$$

$$\begin{aligned} & \bar{U}_{a^*} \frac{\partial T'_{a^*}}{\partial x_*} + \frac{\partial \psi'_{a^*}}{\partial Y_*} \frac{\partial \bar{T}_{a^*}}{\partial x_*} + \bar{v}_{a^*} \frac{\partial T'_{a^*}}{\partial Y_*} - \frac{\partial \psi'_{a^*}}{\partial x_*} \frac{\partial \bar{T}_{a^*}}{\partial Y_*} \\ &= \frac{1}{\text{Pr}_a Gr_a^{1/4}} \left(\frac{\partial^2 T'_{a^*}}{\partial x_*^2} + \frac{\partial^2 T'_{a^*}}{\partial Y_*^2} \right). \end{aligned} \quad (31)$$

We assume ψ'_{a^*} and T'_{a^*} to be

$$\begin{aligned} \psi'_{a^*} &= f_a(Y_*) \xi_{k^*} \exp[\sigma + ikx], \\ T'_{a^*} &= H_a(Y_*) \bar{G}_{a^*} \xi_{k^*} \exp[\sigma + ikx], \end{aligned} \quad (32)$$

where f_a and H_a are dimensionless disturbance amplitude functions, and $\xi_{k^*} = \xi_k / \delta_0$. Substituting (32) into (30) and (31), we obtain the following differential equations for the functions f_a and H_a :

$$\begin{aligned} \frac{d^4 f_a}{dY_*^4} &= \bar{v}_{a^*} \frac{d^3 f_a}{dY_*^3} + \left(2\mu_a^2 + i\mu_a Gr_a^{1/4} \bar{U}_{a^*} \right) \frac{d^2 f_a}{dY_*^2} \\ & - \left(\mu_a^2 \bar{v}_{a^*} + \frac{\partial^2 \bar{v}_{a^*}}{\partial Y_*^2} \right) \frac{df_a}{dY_*} \\ & - \left\{ \mu_a^4 + i\mu_a Gr_a^{1/4} \left(\mu_a^2 \bar{U}_{a^*} + \frac{d^2 \bar{U}_{a^*}}{dY_*^2} \right) \right\} f_a \end{aligned}$$

$$- \bar{G}_{a^*} \frac{dH_a}{dY_*} \sin \theta + i\mu_a \bar{G}_{a^*} H_a \cos \theta, \quad (33)$$

$$\begin{aligned} \frac{d^2 H_a}{dY_*^2} &= \text{Pr}_a \bar{v}_{a^*} \frac{dH_a}{dY_*} + \left(\mu_a^2 + i\mu_a \text{Pr}_a Gr_a^{1/4} \bar{U}_{a^*} \right) H_a \\ & + \text{Pr}_a / \bar{G}_{a^*} \frac{\partial \bar{T}_{a^*}}{\partial X_*} \frac{df_a}{dY_*} - i\mu_a \text{Pr}_a Gr_a^{1/4} / \bar{G}_{a^*} \frac{\partial \bar{T}_{a^*}}{\partial Y_*} f_a, \end{aligned} \quad (34)$$

where $\mu_a = k\delta_0$, and we have neglected the terms $\partial^2 \bar{U}_{a^*} / \partial x_*^2$, $\partial^2 \bar{v}_{a^*} / \partial x_*^2$ and $\partial^2 \bar{T}_{a^*} / \partial x_*^2$ in (30) and (31) because the dependence of the mean velocity profiles \bar{U}_{a^*} , \bar{v}_{a^*} and \bar{T}_{a^*} on x_* is very small. Since the dependence of \bar{U}_{a^*} and \bar{v}_{a^*} on X_* is small, we solve (33) and (34) with respect to Y_* for a given values of Gr_a and X_* numerically with the boundary conditions $df_a / dY_* |_{Y_*=0} = -u_{a0} / \delta_*$, $f_a |_{Y_*=0} = 0$, $df_a / dY_* |_{Y_*=\delta_*} = 0$, and $f_a |_{Y_*=\delta_*} = 0$ obtained from Eq. (14), and $H_a |_{Y_*=0} = 1$ and $H_a |_{Y_*=\delta_*} = 0$. Here we define the perturbed part of the air temperature gradient at the water-air surface as

$$G'_a \equiv \frac{h_0}{\delta_0} \left(- \frac{dH_a}{dY_*} \Big|_{Y_*=0} \right). \quad (35)$$

F. Equations of perturbed part of velocity and temperature in the water film

We briefly summarize equations and boundary conditions for the amplitudes of the perturbed part of the stream function and temperature in the water film with some modifications. We note that the amplitudes $F_l(y)$ and $g_l(y)$ in (20) are expressed as $F_l(y) = u_{l0} f_l(y) \zeta_k$ and $g_l(y) = H_l(y) \bar{G}_l \zeta_k$ [2], where $u_{l0} = h_0^2 g \sin \theta / (2\nu_l)$ is the surface velocity of the water film. The unperturbed temperature gradient is given by $\bar{G}_l \equiv -d\bar{T}_l / dy |_{y=0} = (T_{sl} - T_{la}) / h_0$ under the assumption of a linear temperature distribution in the water film. Here T_{sl} and T_{la} are temperatures at the ice-water interface and water-air surface.

From the perturbed parts of (1) and (2), f_l is governed by the Orr-Sommerfeld equation [2]:

$$\begin{aligned} \frac{d^4 f_l}{dy_*^4} &= \left(2\mu_l^2 + i\mu_l \text{Re}_l \bar{U}_{l^*} \right) \frac{d^2 f_l}{dy_*^2} \\ & - \left\{ \mu_l^4 + i\mu_l \text{Re}_l \left(\mu_l^2 \bar{U}_{l^*} + \frac{d^2 \bar{U}_{l^*}}{dy_*^2} \right) \right\} f_l, \end{aligned} \quad (36)$$

where $y_* = y / h_0$, $\mu_l = kh_0$ and $\bar{U}_{l^*} = -(2y_* - y_*^2)$ is the velocity distribution in the water film in the unperturbed state. $\text{Re}_l \equiv u_{l0} h_0 / \nu_l = 3Q / (2l\nu_l)$ is the Reynolds number. From (10)-(13), using the relation $\xi_k = -(f_l |_{y_*=1} / \bar{U}_{l^*} |_{y_*=1}) \zeta_k$ for the amplitude between the water-air surface and ice-water interface [2], the boundary conditions for f_l can be expressed as [2]:

$$\begin{aligned}
 f_l|_{y^*=0} &= 0, \\
 \left. \frac{df_l}{dy^*} \right|_{y^*=0} &= -\left. \frac{d\bar{U}_{l^*}}{dy^*} \right|_{y^*=0}, \\
 \left. \frac{d^2 f_l}{dy^{*2}} \right|_{y^*=1} &= \left(\left. \frac{d^2 \bar{U}_{l^*}}{dy^{*2}} \right|_{y^*=1} \bar{U}_{l^*}|_{y^*=1} - \mu_l^2 \right) f_l|_{y^*=1}, \\
 \left. \frac{d^3 f_l}{dy^{*3}} \right|_{y^*=1} &= \left(i\mu_l \text{Re}_l + 3\mu_l^2 \right) \left. \frac{df_l}{dy^*} \right|_{y^*=1} - i(\alpha / \bar{U}_{l^*}|_{y^*=1}) f_l|_{y^*=1}, \quad (37)
 \end{aligned}$$

where $\alpha = 2(\cot \theta)\mu_l + 2/\sin \theta (a/h_0)^2 \mu_l^3$ is related to the restoring force due to the surface tension and gravity force, which act on the water-air surface [5].

The perturbed part of (9) yields the equation for H_l [2]:

$$\frac{d^2 H_l}{dy^{*2}} = \left(\mu_l^2 + i\mu_l \text{Pe}_l \bar{U}_{l^*} \right) H_l - i\mu_l \text{Pe}_l \frac{d\bar{T}_{l^*}}{dy^*} f_l, \quad (38)$$

where $\bar{T}_{l^*}(y^*) \equiv (\bar{T}_l(y^*) - T_{sl}) / (T_{sl} - T_{la})$ is the temperature distribution in the water film in the unperturbed state, and $\text{Pe}_l \equiv u_{l0} h_0 / \kappa_l = 3Q / (2l\kappa_l)$ is the Peclet number.

Since the direction of the x axis in Fig. 1 is opposite to that in previous papers [2]-[4], we note that the sign of \bar{U}_{l^*} in this paper is also opposite. Linearization of (17) at $y = h_0$ yields, to the first order in ξ_k ,

$$H_l|_{y^*=1} = -f_l|_{y^*=1} / \bar{U}_{l^*}|_{y^*=1}. \quad (39)$$

Linearization of (18) at $y = h_0$ yields, to the first order in ξ_k ,

$$dH_l / dy^*|_{y^*=1} = G'_a f_l|_{y^*=1} / \bar{U}_{l^*}|_{y^*=1}. \quad (40)$$

F. Dispersion relation

From the perturbed parts of (15) and (16), the real and imaginary parts of the dispersion relation for the perturbation of the ice-water interface give the dimensionless amplification rate $\sigma_*^{(r)} \equiv \sigma^{(r)} / (\bar{V} / h_0)$ and the dimensionless phase velocity $v_{p^*} \equiv -\sigma^{(i)} / (k\bar{V})$, respectively,

$$\sigma_*^{(r)} = -\left. \frac{dH_l^{(r)}}{dy^*} \right|_{y^*=0} + n\mu_l \left(H_l^{(r)}|_{y^*=0} - 1 \right), \quad (41)$$

$$v_{p^*} = -\frac{1}{\mu_l} \left(-\left. \frac{dH_l^{(i)}}{dy^*} \right|_{y^*=0} + n\mu_l H_l^{(i)}|_{y^*=0} \right), \quad (42)$$

where $n = K_s / K_l = 3.96$ is the ratio of the thermal conductivity of ice to that of water, $H_l^{(r)}$ and $H_l^{(i)}$ are the real and imaginary parts of H_l .

III. RESULTS

For the water supply rate per width $Q/l = 50$ [(ml/h)/cm] and the angle $\theta = \pi/2$, Fig. 3 (a) shows the dimensionless amplification rate $\sigma_*^{(r)} \equiv \sigma^{(r)} / (\bar{V} / h_0)$ versus dimensionless wave number $\mu_a = k\delta_0$. We determine the wavelength from

the value of μ_a at which $\sigma_*^{(r)}$ acquires a maximum value for a given Q/l and θ . In the presence of an airflow, $\sigma_*^{(r)}$ acquires a maximum value at $\mu_a = 3.1$ (solid line). Since the wave number k is normalized by δ_0 , the corresponding wavelength is 0.94 cm from $\lambda = 2\pi\delta_0 / \mu_a$. Here we have used $\delta_0 = 4.6$ mm estimated from two parameters $L_0 = 1.0$ m and $\Delta T_a = 10^\circ \text{C}$. At $\mu_a = 3.1$, $v_{p^*} = 0.28$ as represented by the solid line in Fig. 3 (b). While, in the absence of airflow, $\sigma_*^{(r)}$ also acquires a maximum value at $\mu_a = 3.1$ (dashed line). At this value, $v_{p^*} = 0.61$ is represented by the dashed line in Fig. 3 (b). It is found that the maximum value of $\sigma_*^{(r)}$ in the presence of airflow is greater than the maximum in the absence of airflow. This indicates that the natural convection airflow enhances the destabilization of the ice-water interface compared to thermal conduction.

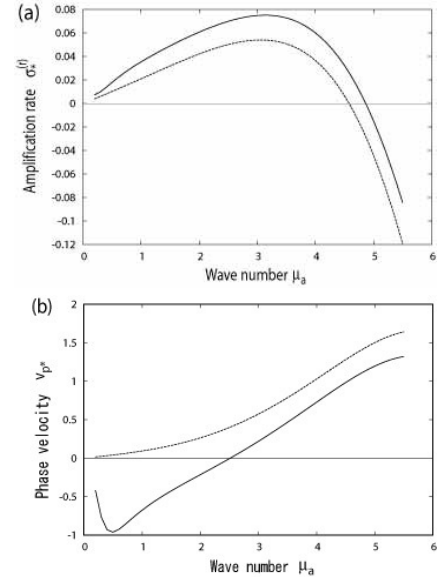


Fig. 3. For $Q/l = 50$ [(ml/h)/cm] and $\theta = \pi/2$, (a) dimensionless amplification rate $\sigma_*^{(r)} = \sigma^{(r)} / (\bar{V} / h_0)$ versus dimensionless wave number $\mu_a = k\delta_0$; (b) dimensionless phase velocity $v_{p^*} = -\sigma^{(i)} / (k\bar{V})$ versus dimensionless wave number μ_a . Solid lines indicate the presence of airflow, and dashed lines indicate the absence of airflow.

It is remarkable that the wavelengths of ripples are almost the same in both cases. When determining the wavelength, we used $\delta_0 = 4.6$ mm. It should be noted that, however, the wavelength is almost the same for other values of δ_0 estimated from different values of ΔT_a , as shown in Table I. This indicates that the wavelengths of ripples on icicles are almost independent of ambient air temperature. In other words, the wavelengths are almost independent of the length scale δ_0 . On the other hand, there is considerable difference for v_{p^*} , which is sensitive to the parameters that characterize the

thermal boundary layer, as shown in Table I. In the absence of airflow, $v_{p*} > 0$ for all modes, as shown in Fig. 3 (b). While in the presence of airflow, v_{p*} has negative values for some unstable long wavelength modes. The sign of v_{p*} changes from negative to positive at $\mu_a = 2.5$.

We note that the mean growth rates \bar{V} of ice in Table I is less than the measured values in the experiments [11] by one order of magnitude. In those experiments, there were large temperature fluctuations. Larger heat transfer mechanisms need to be considered, instead of heat transfer due to natural convection airflow.

TABLE I

The growth rate of ice, \bar{V} , the temperature of the water-air surface, T_{la} , the unit of length to characterize the boundary layer thickness, δ_0 , the wavelength of ripple, λ , the dimensionless phase velocity of ripple, v_{p*} , for respective ambient temperatures T_∞ .

T_∞ (° C)	\bar{V} (mm/h)	T_{la} ($\times 10^{-3}$ ° C)	δ_0 (mm)	λ (mm)	v_{p*}
-5	0.10	1.5	5.5	9.4	0.34
-10	0.24	3.6	4.6	9.4	0.27
-15	0.40	6.0	4.2	9.1	0.28
-20	0.58	8.6	3.9	9.1	0.25

IV. SUMMARY AND DISCUSSION

Although the growth rate of icicle radius and the magnitude of ripple movement depend on parameters to characterize the airflow in the thermal boundary layer ahead of the ice surface, the wavelengths of ripples on icicles in the presence of natural convection airflow are almost the same as those in the absence of airflow.

Even if we take into account the natural convection airflow, as long as the flow of water film is driven by gravity only, the velocity profile in the water film remains $\bar{U}_{l*} = -(2y_* - y_*^2)$, which is derived from the no-slip and the free shear stress boundary conditions at the ice-water interface and water-air surface, respectively. If an aerodynamic force acts on the water-air surface, the boundary conditions (12) and (13) must be modified. As a result, the unperturbed profile \bar{U}_{l*} changes from the above half-parabolic form to $\bar{U}_{l*} = -\{(2y_* - y_*^2) - \bar{\tau}_a / (\tilde{\mu}_l \mu_{l0} / h_0) y_*\}$, where $\bar{\tau}_a = \tilde{\mu}_a \partial \bar{U}_a / \partial y |_{y=h_0}$ is the unperturbed part of shear stress applied at the water-air surface due to the airflow \bar{U}_a , $\tilde{\mu}_l$ and $\tilde{\mu}_a$ being the viscosity of water and air, respectively. Therefore, \bar{U}_{l*} , Re_l and Pe_l in (36)-(40) are all modified. In the absence of airflow, the wavelength was approximately determined from the formula: $\lambda \approx 2\pi(a^2 h_0 Pe_l / 3)^{1/3}$. If shear stress due to airflow is exerted on the water-air surface, the wavelength should be influenced by the airflow.

Based on these considerations, we have to develop the theoretical framework and numerical method to deal with ice and snow accretion on transmission line cables or other equipment under wet conditions, in which air flow, impinging water droplets motion and a supercooled water film motion driven by gravitational and aerodynamic forces, surface tension, and heat conduction through the ice and snow into the object of cylindrical or arbitrary shape must be taken into account simultaneously. Such more complicated situations and the resulting morphological instability of the ice-water interface are under study.

V. ACKNOWLEDGEMENTS

This work was carried out within the framework of NSERC/Hydro-Quebec Industrial Chair on Atmospheric Icing of Power Network Equipment (CIGELE) and the Canada Research Chair on Engineering of Power Network Atmospheric Icing (INGIVRE) at Universite du Quebec a Chicoutimi. The authors would like to thank the CIGELE partners (Hydro-Quebec, Hydro One, Reseau Transport d'Electricite (RTE) and Electricite de France (EDF), Alcan Cable, K-Line Insulators, Tyco Electronics, Dual-ADE, and FUQAC) whose financial support made this research possible.

VI. References

- [1] L. Makkonen and E. P. Lozowski, "Numerical modelling of icing on power network equipment," in *Atmospheric Icing of Power Networks* edited by M. Farzaneh, Berlin : Springer, 2008.
- [2] K. Ueno, "Pattern formation in crystal growth under parabolic shear flow," *Phys. Rev. E*, Vol. 68, 021603, 2003.
- [3] K. Ueno, "Pattern formation in crystal growth under parabolic shear flow II," *Phys. Rev. E*, Vol. 69, 051604, 2004.
- [4] K. Ueno, "Characteristics of the wavelength of ripples on icicles," *Phys. Fluids*, Vol. 19, 093602, 2007.
- [5] T. B. Benjamin, "Wave formation in laminar flow down an inclined plane," *J. Fluid Mech*, Vol. 2, pp. 554-574, 1957.
- [6] L. Landau and E. Lifschitz, *Fluid Mechanics*, London : Pergamon Press, 1959.
- [7] N. Maeno, L. Makkonen, K. Nishimura, K. Kosugi, and T. Takahashi, "Growth rate of icicles," *J. Glaciol*, Vol. 40, pp.319-326, 1984.
- [8] H. Schlichting and K. Gersten, *Boundary Layer Theory*, Berlin: Springer, 1999.
- [9] M. B. Short, J. C. Baygents, and R. E. Goldstein, "A free-boundary theory for the shape of the ideal dripping icicle," *Phys. Fluids*, Vol. 18, 083101, 2006.
- [10] J. P. Holman, *Heat Transfer*, New York: McGraw-Hill, 1990.
- [11] K. Ueno, M. Farzaneh, and S. Yamaguchi, "Comparison of Theoretical Models of Ripple Formation on the Surface of Icicles with Experiments," in *Proc. of 13th International Workshop on Atmospheric Icing on Structures*, Andermatt, Switzerland, 2009.